

Growth of inertia–gravity waves in sheared inertial currents

K. B. WINTERS

Scripps Institution of Oceanography, University of California San Diego,
9500 Gilman Drive, La Jolla, CA 92093-0209, USA

(Received 12 April 2007 and in revised form 10 January 2008)

The linear stability of inviscid non-diffusive density-stratified shear flow in a rotating frame is considered. A temporally periodic base flow, characterized by vertical shear S , buoyancy frequency N and rotation frequency f , is perturbed by infinitesimal inertia–gravity waves. The temporal evolution and stability characteristics of the disturbances are analysed using Floquet theory and the growth rates of unstable solutions are computed numerically. The global structure of solutions is addressed in the dimensionless parameter space $(N/f, S/f, \phi)$ where ϕ is the wavenumber inclination angle from the horizontal for the wave-like perturbations. Both weakly stratified rapidly rotating flows ($N < f$) and strongly stratified slowly rotating flows ($N > f$) are examined. Distinct families of unstable modes are found, each of which can be associated with nearby stable solutions of periodicity T or $2T$ where T is the inertial frequency $2\pi/f$. Rotation is found to be a destabilizing factor in the sense that stable non-rotating shear flows with $N^2/S^2 > 1/4$ can be unstable in a rotating frame. Moreover, instabilities by parametric resonance are found associated with free oscillations at half and integer multiples of the inertial frequency.

1. Introduction

The stability of density-stratified shear flow in a rotating frame is investigated using linear stability theory. In the non-rotating limit, the stability of time-independent stratified shear flows has been extensively studied and fundamental theorems have been derived. The principal result of interest here is the Miles–Howard (Miles 1961; Howard 1961) sufficient condition for stability which states that if $Ri = N^2/S^2$ is everywhere greater than $1/4$, then the flow is stable. Here N is the buoyancy frequency and S is the vertical shear, both of which may vary with height z . This result however, and indeed the classical normal mode approach to stability analysis (see e.g. Drazin & Reid 1981; Chandrasekhar 1961), are not applicable to time-dependent shear flows. A fundamental yet unanswered question is: *what is the effect of rotation on the basic stability properties of stratified shear flows?*

If the base flow is periodic, parametric instabilities related to resonance between infinitesimal, free wave perturbations and half or integer multiples of the forcing frequency are possible and these instabilities have been observed experimentally for both surface (Faraday 1831) and internal gravity waves (Bennielli & Sommeria 1998). The stability of time-periodic flows can be analysed using Floquet theory for periodic ordinary differential equations (Ince 1956; Hochstadt 1961; Bender & Orszag 1978). The Floquet approach has been used to examine the stability properties of internal gravity waves in a non-rotating frame and parametric instabilities have been identified

for all wave amplitudes and, in particular, for arbitrarily large values of Ri (Mied 1976; Drazin 1977; Lombard & Riley 1996), Majda & Shefter 1998).

Numerical investigations of parametrically unstable internal waves have focused on both the early stages of the instability for which linear stability theory is applicable and also on the nature of the fully developed flow, energy transfer mechanisms, implications for a laminar to turbulent transition and particle dispersion and mixing (Bouruet-Aubertot *et al.* 1995; Lombard & Riley 1996; Bouruet-Aubertot *et al.* 2001).

In this work, we consider time-dependent shear flows in which the time dependence is periodic, arising from rotational effects. The primary motivation is geophysical and in this context we seek to determine the stability of sheared horizontal inertial currents. There are three fundamental time scales in the problem, defined by N , S , and the rotation frequency f , and the stability of infinitesimal inertia-gravity waves is related to these frequencies through resonance conditions. Growth rates are determined numerically and families of unstable solutions are identified as a function of the parameters defining the inertial shear flow and the infinitesimal test waves. The stability problem is analysed for both the weakly stratified rapidly rotating regime where $N < f$ and the strongly stratified slowly rotating limit $N > f$ which characterizes many oceanic flows. Two-dimensional numerical simulations are used to verify the stability analysis and to explore the nature of the flow once the perturbations reach finite amplitude.

2. Mathematical model

Our starting point is the Boussinesq equations for a density-stratified fluid, expanded about a depth-dependent ambient state consisting of a stable potential density profile $\bar{\rho}(z)$ and a sheared inertial current $[\mathcal{U}, \mathcal{V}] = U_0(z)[\cos(ft), -\sin(ft)]$. The horizontal velocity is written as $[u, v] = [\mathcal{U}, \mathcal{V}] + [u', v']$ where the perturbation $[u', v']$ is taken to be sufficiently small in magnitude so that, to leading order, we neglect terms that are quadratic in the perturbation variables. Here z is the vertical coordinate (positive upward), x and y are the horizontal coordinates, t is time, and f is the rotation frequency. The linearized equations for small perturbations from the basic state are

$$\frac{\partial u'}{\partial t} - fv' + \mathcal{U}(z, t) \frac{\partial u'}{\partial x} + \mathcal{V}(z, t) \frac{\partial u'}{\partial y} + w' \mathcal{U}_z(z, t) = -\frac{1}{\rho_0} \frac{\partial p'}{\partial x}, \quad (2.1)$$

$$\frac{\partial v'}{\partial t} + fu' + \mathcal{U}(z, t) \frac{\partial v'}{\partial x} + \mathcal{V}(z, t) \frac{\partial v'}{\partial y} + w' \mathcal{V}_z(z, t) = -\frac{1}{\rho_0} \frac{\partial p'}{\partial y}, \quad (2.2)$$

$$\frac{\partial w'}{\partial t} + \mathcal{U}(z, t) \frac{\partial w'}{\partial x} + \mathcal{V}(z, t) \frac{\partial w'}{\partial y} + \frac{g}{\rho_0} \rho' = -\frac{1}{\rho_0} \frac{\partial p'}{\partial z}, \quad (2.3)$$

$$\frac{\partial \rho'}{\partial t} + \mathcal{U}(z, t) \frac{\partial \rho'}{\partial x} + \mathcal{V}(z, t) \frac{\partial \rho'}{\partial y} + w' \frac{d\bar{\rho}}{dz} = 0, \quad (2.4)$$

$$\frac{\partial u'}{\partial x} + \frac{\partial v'}{\partial y} + \frac{\partial w'}{\partial z} = 0, \quad (2.5)$$

It is convenient to shift to a time-dependent horizontally Lagrangian frame by introducing the coordinate transformations:

$$\xi = x - \int^t \mathcal{U} dt' = x - \frac{U_0(z)}{f} \sin(ft), \quad (2.6)$$

$$\eta = y - \int^t \mathcal{V} dt' = y - \frac{U_0(z)}{f} \cos(ft), \quad (2.7)$$

In terms of these coordinates we have

$$\frac{\partial u'}{\partial t} - f v' + \mathcal{U}_z w' = -\frac{1}{\rho_0} \frac{\partial p'}{\partial \xi}, \quad (2.8)$$

$$\frac{\partial v'}{\partial t} + f u' + \mathcal{V}_z w' = -\frac{1}{\rho_0} \frac{\partial p'}{\partial \eta}, \quad (2.9)$$

$$\frac{\partial w'}{\partial t} + \frac{g}{\rho_0} \rho' = -\frac{1}{\rho_0} \left(\frac{\partial p'}{\partial z} + \frac{\dot{\mathcal{U}}_z}{f^2} \frac{\partial p'}{\partial \xi} + \frac{\dot{\mathcal{V}}_z}{f^2} \frac{\partial p'}{\partial \eta} \right), \quad (2.10)$$

$$\frac{\partial \rho'}{\partial t} + w' \frac{d\bar{\rho}}{dz} = 0, \quad (2.11)$$

$$\frac{\partial u'}{\partial \xi} + \frac{\partial v'}{\partial \eta} + \frac{\partial w'}{\partial z} + \frac{\dot{\mathcal{U}}_z}{f^2} \frac{\partial w'}{\partial \xi} + \frac{\dot{\mathcal{V}}_z}{f^2} \frac{\partial w'}{\partial \eta} = 0. \quad (2.12)$$

3. Time-dependent normal mode analysis

We now seek solutions to these equations in the form of time-dependent normal modes with respect to the transformed variables. Noting that there is no preferred horizontal direction, we consider the time dependence of two-dimensional wave-like disturbances of the form

$$p'(\xi, z, t) = \hat{p}'(t) e^{i(k\xi + mz)}, \quad (3.1)$$

assuming similar forms for the other primed variables.

Substituting into Eq. 2.10 we find

$$\hat{p}'(t) = \frac{i\rho_0}{(m + k\dot{\mathcal{U}}_z/f^2)} \left(\frac{\partial \hat{w}'}{\partial t} + \frac{g}{\rho_0} \hat{\rho}' \right), \quad (3.2)$$

and differentiating (2.9) with respect to ξ and combining with Eq. (2.12) gives

$$\frac{\partial \hat{v}'}{\partial t} = f \frac{m}{k} \hat{w}'. \quad (3.3)$$

Using (3.2) in (2.8), differentiating with respect to ξ and using continuity (2.12), gives

$$-\left(\left(\frac{m}{k} + \frac{\dot{\mathcal{U}}_z}{f^2} \right)^2 + 1 \right) \frac{\partial \hat{w}'}{\partial t} + 2 \left(\frac{m}{k} + \frac{\dot{\mathcal{U}}_z}{f^2} \right) \mathcal{U}_z w - f \left(\frac{m}{k} + \frac{\dot{\mathcal{U}}_z}{f^2} \right) v - \frac{g}{\rho_0} \rho' = 0. \quad (3.4)$$

Let $N^2 = -(g/\rho_0)(d\bar{\rho}/dz)$, taken hereafter to be independent of z . To simplify notation, let $\tan \phi = m/k$ parameterize the wavenumber vector orientation of infinitesimal disturbances. Let $\mathcal{S} = (dU_0/dz)/f$ be the dimensionless ambient shear and $\mathcal{N} = N/f$, both taken as depth-independent constants. Denoting $\Omega(\tau) = \tan \phi - \mathcal{S} \sin(\tau)$, with dimensionless time $\tau = ft$, and using (2.11) and (3.3) to relate v and ρ' , the stability problem can be expressed as

$$\frac{\partial}{\partial \tau} \begin{bmatrix} \hat{w} \\ \hat{\rho} \end{bmatrix} = \begin{bmatrix} 2 \frac{\mathcal{S}\Omega}{1 + \Omega^2} \cos(\tau) & -\frac{\mathcal{N}^2 + \Omega \tan \phi}{1 + \Omega^2} \\ 1 & 0 \end{bmatrix} \begin{bmatrix} \hat{w} \\ \hat{\rho} \end{bmatrix}. \quad (3.5)$$

Here \hat{w} is the dimensionless, time-varying amplitude of the vertical velocity perturbation, scaled by fL , $\hat{\rho}$ is the corresponding amplitude of the density

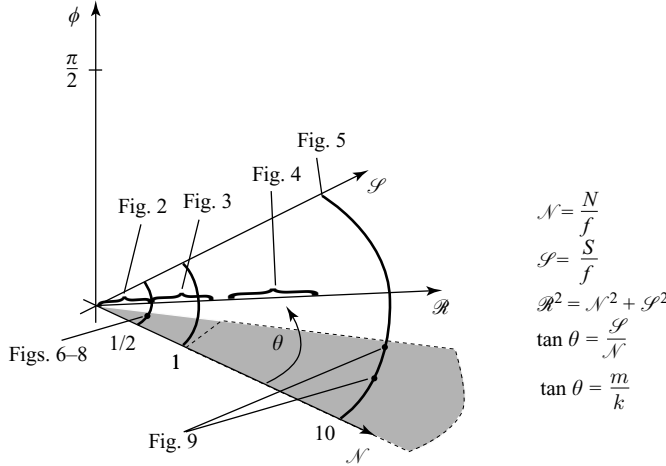


FIGURE 1. Dimensionless parameter space for the linear stability problem. The base state is defined by the frequencies N and f parameterized by \mathcal{R} and θ . The inclination angle of the perturbation wavenumber is given by ϕ .

perturbation, scaled by $L|d\bar{\rho}/dz|$ and L is taken to be a vertical length scale over which the ambient flow properties \mathcal{N} and \mathcal{S} are taken as constant.

It is convenient here to introduce polar coordinates \mathcal{R} and θ where $\mathcal{N} = \mathcal{R} \cos(\theta)$ and $\mathcal{S} = \mathcal{R} \sin(\theta)$. We seek to determine (i) the parameter values (\mathcal{R}, θ) describing sheared inertial currents for which infinitesimal perturbations with wavenumber orientation ϕ experience exponential growth in time and (ii) the corresponding growth rates. Because the coefficient matrix in (3.5) is 2π -periodic with respect to τ , we will use Floquet theory to determine growth rates for discrete values of \mathcal{R} as a function of (θ, ϕ) . A schematic of the parameter space is shown in figure 1. The portion of this space, projected onto the $\phi = 0$ plane, where $N^2/S^2 > 4$ is shown schematically via shading. The dashed line indicates the region where, in addition, $N/f > 1$, which is generally the case for stably stratified flows in the oceans and atmosphere, though there may also be weakly stratified geophysical flows of interest, perhaps near boundaries and/or at high latitudes where $N/f < 1$. As we will see shortly, there are special values, $\mathcal{R} = \{1/2, 1\}$, where the structure of the set of unstable solutions changes and these values are indicated by heavy curves. In §6, we show the results of stability calculations in the (θ, ϕ) -plane for several values of \mathcal{R} as indicated by figure number. In §7, the results of two-dimensional direct numerical simulations are shown for the parameter values indicated with filled circles.

4. Unsheared limit: $\mathcal{S} = \theta = 0$

Before examining the general problem (3.5) however, it is useful to examine the limit $\mathcal{S} = 0$. When $\mathcal{S} = 0$, $\Omega = \tan \phi$ and (3.5) can be reduced to a single second-order ordinary differential equation for $\hat{w}(\tau)$:

$$\frac{d^2}{d\tau^2} \hat{w} + \frac{\mathcal{N}^2 + \tan^2 \phi}{1 + \tan^2 \phi} \hat{w} = 0, \quad (4.1)$$

with purely oscillatory solutions $\hat{w}(\tau) = e^{i\omega_* \tau}$ and the standard dispersion relation $\omega_*^2 = (\mathcal{N}^2 + \tan^2 \phi)/(1 + \tan^2 \phi)$. When $\mathcal{N} > 1$, the dimensionless frequency satisfies

$1 \leq \omega_* \leq \mathcal{N}$ whereas for $\mathcal{N} < 1$, we have $\mathcal{N} \leq \omega_* \leq 1$. In either case, the dimensionless inertial period T is equal to 2π .

Transforming back to the original, dimensional coordinates (x, z, t) gives

$$w = \exp(i(kx + mz - \frac{kU_0}{f} \sin(ft) - \omega_0 t)) \quad (4.2)$$

where $\omega_0^2 = (k^2 N^2 + m^2 f^2)/(k^2 + m^2)$. The depth-independent inertially oscillating current modulates the intrinsic frequency of infinitesimal internal waves by Doppler shifting as the current rotates into and out of alignment with the horizontal component of the wavevector. In general, the solutions of (4.2) comprise a continuous spectrum of non-periodic waves along the $\theta = 0$ axis.

Within this spectrum however, there are discrete periodic solutions. Periodicities of T and $2T$ are possible when $\omega_* = \{1, 2, 3, \dots\}$ and $\omega_* = \{\frac{1}{2}, \frac{3}{2}, \frac{5}{2}, \dots\}$ respectively. As we will see, the identification of waves of critical frequency when $\mathcal{S} = 0$, i.e. free waves with periodicities matching the inertial period or its subharmonic, is useful in interpreting the numerically determined stability characteristics when $\mathcal{S} > 0$. For $\mathcal{N} > 1$ the frequency $\omega_* = \frac{1}{2}$ is subinertial, does not satisfy the dispersion relation, and therefore must be discarded. The remaining frequencies form two distinct sets of periodic waves. Both sets are finite owing to the restriction $\omega_* \leq \mathcal{N}$.

For $\mathcal{N} < 1$ however, superinertial frequencies $\omega_* > 1$ do not satisfy the dispersion relation. Provided that $\mathcal{N} \leq \frac{1}{2}$, there are exactly two periodic solutions with frequencies $\omega_* = \{1, \frac{1}{2}\}$ while for $\frac{1}{2} < \mathcal{N} < 1$ the only periodic solution is a pure inertial flow with $\omega_* = 1$. Thus, for $\mathcal{N} \leq \frac{1}{2}$ there exists exactly one inertia–gravity wave that is resonant with the subharmonic of the inertial frequency. For the special case $\mathcal{N} = \frac{1}{2}$, this critical wave is a pure buoyancy oscillation with strictly vertical displacements. For $\mathcal{N} < \frac{1}{2}$, the wavevector of the critical wave is inclined from the horizontal and the wave motions have both horizontal and vertical components.

5. Floquet analysis

We can exploit the fact that the coefficient matrix in (3.5) is periodic in time. Defining the vector $\boldsymbol{\psi}(\tau) = [\hat{w}(\tau), \hat{\rho}(\tau)]^T$ we rewrite (3.5) as

$$\frac{\partial}{\partial \tau} \boldsymbol{\psi} = \mathbf{A}(\tau) \boldsymbol{\psi}. \quad (5.1)$$

From Floquet theory (see e.g. Ince 1956; Bender & Orszag 1978; Hochstadt 1961) we know that if $\boldsymbol{\Psi} = (\boldsymbol{\psi}_1(\tau), \boldsymbol{\psi}_2(\tau))$ is a matrix with columns composed of two linearly independent solutions of (5.1), then there exists a non-singular matrix of constants \mathbf{K} such that

$$\boldsymbol{\Psi}(\tau + T) = \mathbf{K} \boldsymbol{\Psi}(\tau) \quad (5.2)$$

where $T = 2\pi$ is the fundamental period of the coefficient matrix and $\det(\mathbf{K}) = 1$. Floquet theory also states that there exists at least one solution of the form

$$\boldsymbol{\psi}(\tau) = e^{\mu \tau} \mathbf{p}(\tau) \quad (5.3)$$

where $\lambda_i = e^{\mu_i T}$ $i = 1, 2$ are the eigenvalues of \mathbf{K} and $\mathbf{p}(\tau)$ is a T -periodic vector. The eigenvalues of \mathbf{K} therefore determine the stability of the general solution of (3.5) for a given set of parameter values $(\mathcal{R}, \theta, \phi)$.

Our objective then is to determine the stability properties of solutions in the three-dimensional parameter space defining the ambient inertial current, and stratification

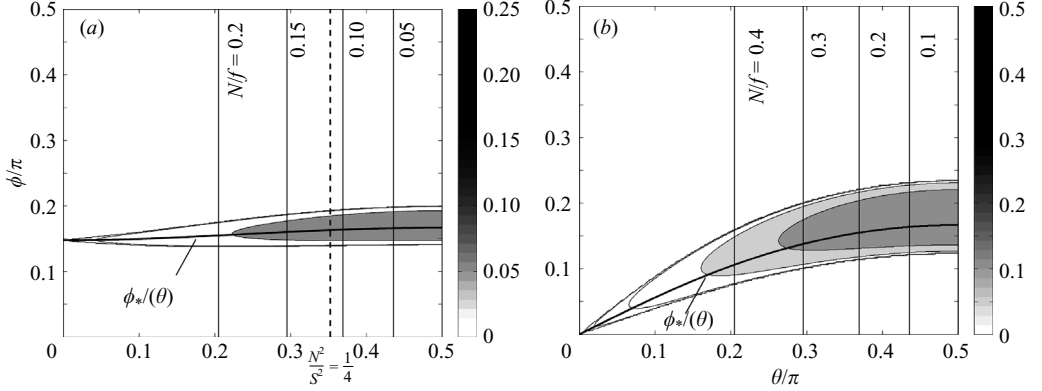


FIGURE 2. Dimensionless growth rates, scaled by f , of unstable modes in the (θ, ϕ) -plane for (a) $\mathcal{R}=0.25$, (b) $\mathcal{R}=0.5$. Values of θ corresponding to discrete values of N/f are indicated in both panels along with the particular value associated with $N^2/S^2=1/4$ ((a) only). The blue curves relate the inclination angle to θ using the unsheared dispersion relation which is formally valid only when $\theta=0$ (see text).

and wavenumber inclination angle of infinitesimal disturbances. By twice integrating (5.1) numerically, from $\tau=0$ to $\tau=T$, using the initial conditions $\boldsymbol{\psi}(0)=[1, 0]^T$ and $\boldsymbol{\psi}(0)=[0, 1]^T$, we can simultaneously determine both $\boldsymbol{\Psi}(T)$ and \mathbf{K} for a given triplet $(\mathcal{R}, \theta, \phi)$. For each pair of integrations, we confirm accuracy by comparing the determinant of the numerically computed \mathbf{K} to the theoretical value of 1, which ensures that the two computed solutions $\boldsymbol{\psi}_i$ are indeed linearly independent. The eigenvalues of \mathbf{K} then determine the stability properties of two linearly independent solutions and therefore of the general solution. Stable and unstable regions of parameter space are separated by transition curves, along which $\mu=0$ and solutions are both stable and periodic with periodicity T or $2T$.

6. Stability diagrams

Growth rates μ were computed numerically by integrating (3.5) in time to generate the 2×2 matrix \mathbf{K} as a function of the background flow parameters $(\mathcal{N}, \mathcal{S})$ and the perturbation wavenumber inclination ϕ . To illustrate the structure of the unstable solutions in this three-dimensional parameter space, the results are displayed in the two-dimensional (θ, ϕ) -plane (see figure 1) for selected values of \mathcal{R} . To understand the somewhat complex structure of the solutions shown for moderate values of \mathcal{R} , it is instructive to first examine the structure for small values and note the changes that occur as \mathcal{R} increases.

6.1. $\mathcal{R} \leq \frac{1}{2}$

We first consider stability diagrams for cases $\mathcal{R} \leq 1/2$ shown in figure 2. Contours of dimensionless growth rates μ are drawn for $\mu = \{10^{-4}, 10^{-3}, 10^{-2}, 0.05, 0.1\}$. In these diagrams, because $(\mathcal{N}, \mathcal{S})$ is given by $\mathcal{R}(\cos(\theta), \sin(\theta))$, N/f decreases from a value of \mathcal{R} when $\theta=0$ to zero when $\theta=\pi/2$. Lines of constant N/f are indicated in each panel. Similarly, the ratio N^2/S^2 decreases with increasing θ . The value $N^2/S^2=1/4$ is indicated in figure 2(a) for reference. For steady parallel shear flows, $N^2/S^2 \leq 1/4$ is a necessary but not sufficient condition for Kelvin–Helmholtz instability. The flows considered here however, are not steady and the $N^2/S^2=1/4$ value has no

formal theoretical significance. Unstable modes are found for both larger and smaller values.

When $\theta=0$, $\mathcal{S}=0$ and we have already identified a continuous spectrum of Doppler-shifted wave solutions. For the case $\mathcal{R}=1/4$ shown in figure 2(a), the unsheared ($\theta=0$) wave with $\phi=\phi_*\approx 0.15\pi$ has a dimensionless frequency of $1/2$ and is the only wave that is $2T$ -periodic. As \mathcal{R} increases, the elevation angle ϕ corresponding to the unsheared wave with $\omega_*=1/2$ decreases. At the critical value $\mathcal{R}=1/2$, $\phi=0$ and the resonant wave is a pure buoyancy oscillation. Figure 2 shows that the $2T$ -periodic waves in the $\mathcal{S}=0$ limit correspond to points on the $\theta=0$ axis bounding regions of instability in the (θ, ϕ) -plane. Within these unstable regions, perturbations have exponential growth rates $\mu > 0$ that increase with increasing θ , i.e. for decreasing ratios N/S . The main result here is that a weakly stratified or rapidly rotating ($N \leq f/2$) sheared inertial current is always unstable. There always exist infinitesimal inertia–gravity wave perturbations that grow exponentially in time. Furthermore, the wavenumber inclination angle of the most unstable perturbation can be estimated using a simple resonance argument matching the periodicity of free waves to the subharmonic of the inertial forcing.

Because \mathcal{N} decreases with increasing θ , the wavenumber elevation angle for an infinitesimal free inertia–gravity wave, $\phi_*(\theta)$, with subharmonic frequency $1/2$ must increase. Using the *unsheared* dispersion relation (without formal justification because \mathcal{S} is not small throughout the figure) and setting $\omega_*=1/2$, $\mathcal{N}=\mathcal{R}\cos(\theta)$ gives

$$\phi_*(\theta) = \tan^{-1} \sqrt{\frac{1 - 4\mathcal{R}^2 \cos^2(\theta)}{3}} \quad (6.1)$$

as shown in the figure. These curves approximately bisect the unstable regions and provide reasonable estimates of ϕ for the most unstable mode, suggesting that the physical mechanism enabling infinitesimal wave-like disturbances to grow in time is related to an approximate resonance between inertia–gravity waves and the subharmonic of the shear forcing frequency.

6.2. $\frac{1}{2} < \mathcal{R} < \frac{3}{2}$

Stability diagrams for $\mathcal{R}=O(1)$ are shown in figure 3. For $1/2 \leq \mathcal{R} < 1$, there is only a narrow range of free wave frequencies $\mathcal{N} \leq \omega_* \leq 1$, all of which are greater than $1/2$ but less than $3/2$. In this region of parameter space, no $2T$ -periodic free waves are possible. Nevertheless, there are unstable regions of parameter space and within these regions, growth rates increase with decreasing N/S . These regions, however, do not shrink to isolated points on the $\theta=0$ axis but rather to points on the $\phi=0$ axis for which perturbation velocities are purely vertical.

The critical intersection values θ_* , however, are not easily recoverable. For $\mathcal{R}=O(1)$, we see that the critical values occur near the intersection of $N/f=1/2$, i.e. where buoyancy oscillations with $\phi=0$ have dimensionless frequencies of $1/2$ and periods of $2T$ but displaced somewhat to the left. Unfortunately, the (3.5) do not reduce to an easily solvable limit on $\phi=0$ axis. To predict the intersection points, it is necessary to determine conditions for $2T$ -periodic solutions with $\phi=0$ but for finite values of \mathcal{S} . Solution of this problem appears to be as difficult as solving the stability problem for arbitrary points in the interior of the (θ, ϕ) -plane. Though we cannot offer an analytical demonstration, it appears that these unstable regions are closely related to those associated with unsheared wave resonances discussed previously. In this case however, the stable $2T$ -periodic solutions involve purely vertical perturbations, transitioning from from the $\theta=0$ axis to the $\phi=0$ axis when \mathcal{R} exceeds $1/2$. We

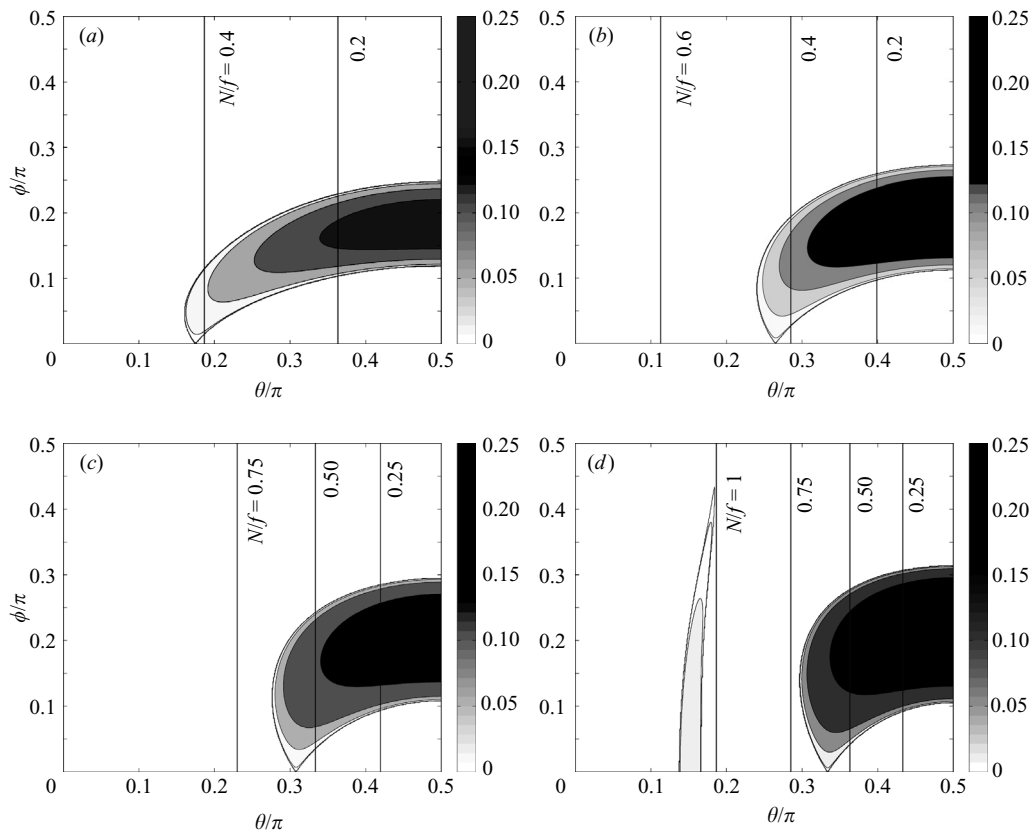


FIGURE 3. Dimensionless growth rates for $\mathcal{R} = (a)$ 0.6, (b) 0.8, (c) 1.0, (d) 1.2.

conjecture that a more complex resonance condition, relating the buoyancy frequency N , the shear frequency S and the subharmonic $f/2$ distinguishes the stable $2T$ -periodic solutions when $\phi = 0$.

As \mathcal{R} increases, there are systematic changes to the character of this family of unstable solutions. Both the $\phi = 0$ intercept θ_* and the maximum growth rate increase with \mathcal{R} . The selectivity mechanism, however, appears to weaken. For any particular value of θ for which unstable solutions exist, increasing \mathcal{R} results in a broader range of unstable inclination angles ϕ . This observation is apparent not only in figure 3 but in the subsequent figures as well.

When $\mathcal{R} > 1$ (figure 3d), a new set of unstable solutions emerges. The unstable region for this set shrinks asymptotically to the point $\phi = \pi/2$, $\theta = \cos^{-1}(1/\mathcal{R})$ corresponding to purely horizontal inertially oscillating disturbances that are unaffected by the ambient shear. In contrast to the unstable modes discussed previously, the region within which these additional modes exist is bounded by stable T -periodic solutions. It is clear from the stability diagram that, compared to the modes bounded by $2T$ -periodic solutions, the growth rates of these solutions are considerably smaller.

Note also that when $\mathcal{R} > 1$, $1 \leq \omega_* \leq \mathcal{R}$ for all values of (θ, ϕ) . The previously distinguished wave frequency $\omega_* = 1/2$ does not satisfy the dispersion relation and no free waves of this frequency are supported. Furthermore, for $1 \leq \mathcal{R} < 3/2$, there are no free wave solutions satisfying $2T$ periodicity.

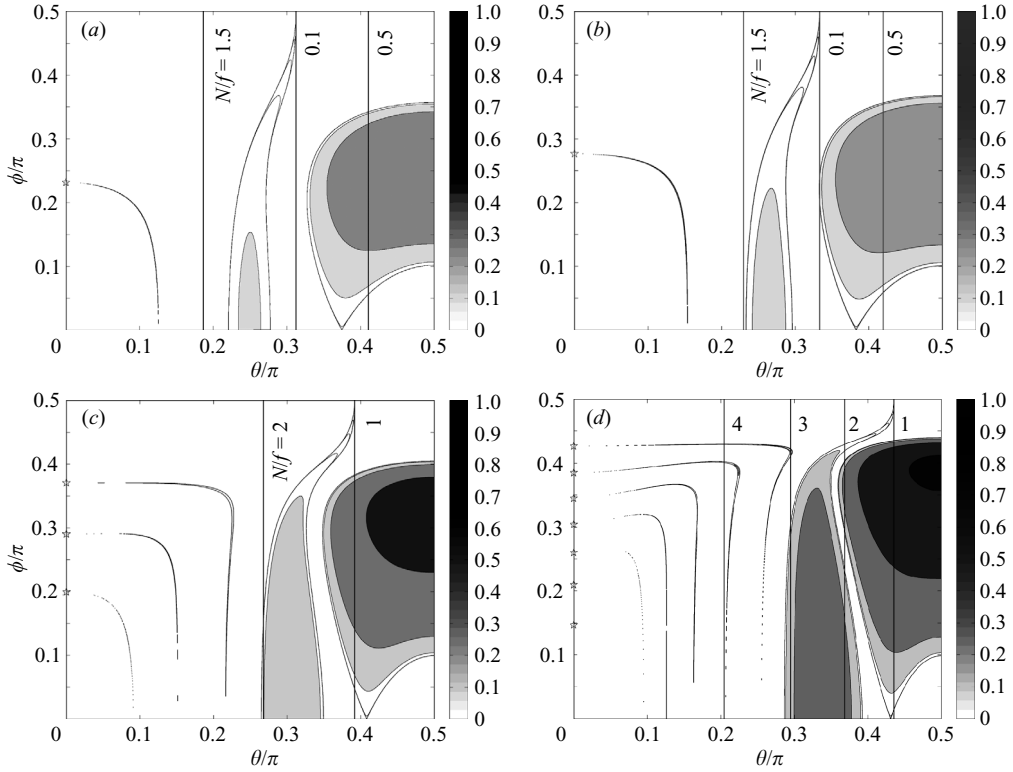


FIGURE 4. Growth rates, $\mathcal{R} = (a) \{1.8, (b) 2, (c) 3, (d) 5\}$. For $\mathcal{R} > 3/2$, additional families of unstable solutions are found. These solutions are associated with the $2T$ -periodic, free wave frequency $\omega_* = 3/2$ (uppermost red star in all panels), $\omega_* = 2$ (uppermost blue star in (b) and (c)), $\omega_* = 5/2$ (second red star from top in (b) and (c)), $\omega_* = 3$ (second blue star in (c)) etc. Though unstable solutions are expected, associated with $\omega_* = 4$ and $9/2$, these solutions were not captured at the resolution used to discretize θ and ϕ for this figure. (A higher resolution analysis is shown in figure 5.)

6.3. $\mathcal{R} > \frac{3}{2}$

For $\mathcal{R} > 3/2$ parts of the (θ, ϕ) -plane have $\mathcal{N} > 3/2$ and, for $\theta = 0$, $2T$ -periodic waves with frequencies $\omega_* = 3/2, 5/2, \dots$ exist provided that $\omega_* \leq \mathcal{R}$. The stability diagram for $\mathcal{R} = 1.8$ is shown in figure 4(a). In this case, the only $2T$ -periodic wave possible is that with $\omega_* = 3/2$. As in the previous cases, associated with the exact $2T$ -periodic solution for $\theta = \mathcal{S} = 0$ is a set of unstable modes for $\mathcal{S} > 0$, though in this case the region of instability intersects both the $\theta = 0$ axis, where the analytical solution is known, and the $\phi = 0$ axis, for which \mathcal{S} is finite and a closed-form solution is not known. Again, we can attempt to estimate the $\phi = 0$ intercept by neglecting \mathcal{S} and calculating the value $\theta = \cos^{-1}(3/2\mathcal{R}) \approx 0.19\pi$ for which pure buoyancy oscillations have a dimensionless frequency of $3/2$, but this overestimates the observed intercept considerably. Again, it appears that \mathcal{S} cannot be ignored and that there exist stable $2T$ -periodic solutions fundamentally influenced by shear.

As \mathcal{R} increases to 2, figure 4(b), no additional distinguished frequencies are possible, but the value of ϕ for which free waves satisfy $\omega_* = 3/2$ moves upward on the $\theta = 0$ axis and the value of θ , for which $\mathcal{N} = 3/2$ moves to the right. The associated region of unstable modes moves correspondingly outward from the origin. Our crude estimate

for the $\phi = 0$ intercept explains the trend as \mathcal{R} increases but, as before, overestimates the intercept itself.

With increasing \mathcal{R} , the contour line $N/f = 1$ moves to the right along with the family of unstable modes that asymptotes to the $\phi = \pi/2$, $\theta = \cos^{-1}(1/\mathcal{R})$ T -periodic solution. Both the size of the unstable region associated with these modes and their maximum growth rates increase. These solutions also exhibit weak mode selectivity. Within this family, for a given θ , growth rates are approximately uniform for a wide range of ϕ less than about 0.35π .

Figure 4(c) shows the results for $\mathcal{R} = 3$. Both the $3/2$ and $5/2$ frequencies are possible here and the ϕ values for the corresponding $2T$ -periodic free waves for $\mathcal{S} = 0$ are indicated in the figure. Also shown is the value for the T -periodic wave with $\omega_* = 2$. Associated with each of these periodic solutions is a distinct region of unstable modes when $\mathcal{S} > 0$. As \mathcal{R} continues to increase, more resonant wave frequencies satisfy the dispersion relation and additional distinct families of unstable modes are seen (figure 4c). In general, with increasing \mathcal{R} , all previously existing families of unstable modes shift to the right and exhibit faster growth rates while additional families of unstable modes make their initial appearance in the lower left portion of the plane. In contrast to both families of unstable solutions discussed previously, these new solutions are both strongly and weakly mode selective, depending on the N/S ratio. For the family of modes associated with a given T - or $2T$ -periodic solution when $S = 0$, only a very narrow range of ϕ yields unstable solutions at smaller values of N/S . As N/S approaches some critical value, however, the instability transitions to a weakly selective one where a broad range of ϕ values grow exponentially.

The size of the regions defining the unstable solutions becomes very small for small values of either θ or ϕ . Moreover, the associated growth rates vanish as the axes are approached. Though we are able to extract the general structure of the instability diagrams and understand qualitatively how the results change as \mathcal{R} increases, it would be computationally demanding to try to recover precise quantitative details of the higher frequency modes for large values of \mathcal{R} . Very high resolution in parameter space is required to resolve the vanishingly thin unstable regions. Furthermore, each growth rate estimate requires numerical integration over a dimensionless time T followed by a calculation of the eigenvalues of the resulting matrix \mathbf{K} . In this regime however, in addition to the slow time evolution, the solutions also oscillate at the higher frequencies associated with the wavenumber inclination ϕ . As these intrinsic frequencies increase, it becomes more and more difficult to integrate over an inertial period to a specified minimum accuracy. Finally, the accuracy requirements increase with frequency because the corresponding growth rates decrease. Figure 5 is the stability diagram for $\mathcal{R} = 10$ computed with a parameter discretization $\Delta\theta = \Delta\phi = 1/15000$.

6.4. Summary of stability results

Linear stability is examined in the parameter space (\mathcal{R}, θ) that uniquely defines the constant dimensionless shear and buoyancy frequencies of an idealized inertial current, normalized by the Coriolis parameter $f > 0$. Floquet theory is used to determine exponential growth rates of infinitesimal disturbances with wavenumber inclination angle ϕ .

Throughout this parameter space, the most unstable modes are found to be associated with $2T$ -periodic solutions, i.e. within distinct regions of parameter space that asymptote to distinct $2T$ -periodic solutions with zero growth rate. This statement

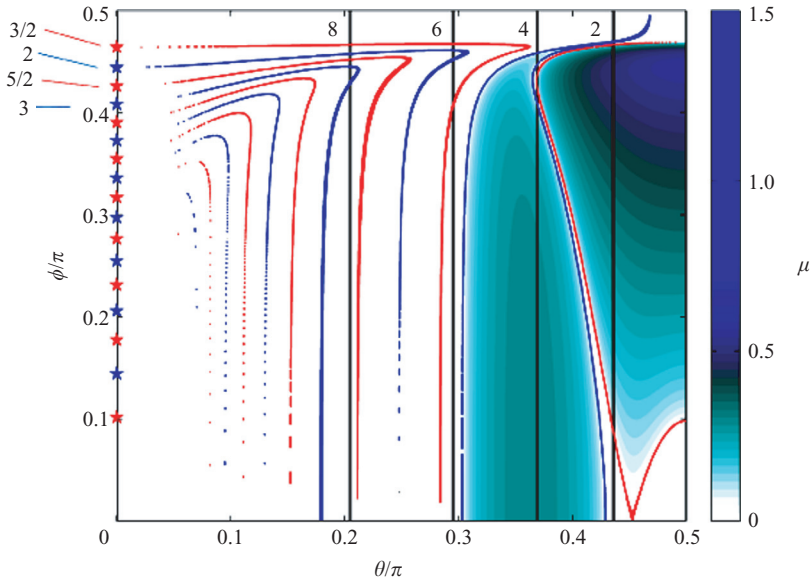


FIGURE 5. Growth rates for the case $\mathcal{R}=10$ are shown in colour. The locations where maximal growth rates satisfy $5 \times 10^{-7} \leq \mu \leq 0.025$ are indicated in red and blue, corresponding to bounding stable solutions of periodicity $2T$ and T respectively. Also shown are the inclination angles ϕ_* corresponding to unsheared resonant wave frequencies using the same colour convention. Only the lowest few frequencies in each set are explicitly labelled. The vertical lines indicate the particular values θ corresponding to N/f values of 8, 6, 4 and 2 as indicated.

is made rigorously for the case $\mathcal{R} \leq 1/2$ where the periodic asymptotic solutions can be expressed in closed form. For $\mathcal{R} > 1/2$, this family of unstable modes no longer intersects the $\mathcal{S}=0$ axis but rather the $\phi=0$ axis, with the intersection point θ increasing with \mathcal{R} . In this case, no closed-form solution has been found and the classification of the solution families is inferred from the numerical results. For \mathcal{R} greater than about 2, this family of unstable solutions exists in a region of parameter space where $N^2/S^2 < 1/4$, though this familiar value has no specific relevance in the context of time-dependent flows considered here. These solutions are generally only weakly mode selective.

In addition to this family, when $\mathcal{R} > 1$, a second family of unstable modes is found. These solutions exhibit an asymptotic association with the particular stable T -periodic inertial solution with $N=f$. The physical interpretation of this result is not clear. For all $\mathcal{R} \geq 1$, the maximum growth rate within this second family of unstable solutions is always less than that found within the first set. For all $\mathcal{R} > 1$ there are always unstable solutions within this family for which $N^2/S^2 > 1/4$. This family of solutions is also weakly mode selective.

As \mathcal{R} increases beyond $3/2$, additional distinct families of unstable solutions are found. These families are associated with the T -periodic dimensionless frequencies $\{1, 2, 3 \dots\}$ and the $2T$ -periodic frequencies $\{3/2, 5/2, 7/2 \dots\}$ for all such frequencies less than \mathcal{R} . The growth rates of these solutions are always smaller than for either of the first two families discussed above and decrease with increasing frequency.

7. Two-dimensional nonlinear evolution

To illustrate the growth of unstable perturbations, solutions to two-dimensional initial value problems are computed numerically. The governing equations are

$$\frac{\partial \mathbf{u}}{\partial t} + \mathbf{u} \cdot \nabla \mathbf{u} + \hat{\mathbf{k}} f \times \mathbf{u} + \frac{g}{\rho_0} \rho = -\frac{1}{\rho_0} \nabla p + \nu \nabla^2 \mathbf{u}, \quad (7.1)$$

$$\frac{\partial \rho}{\partial t} + \mathbf{u} \cdot \nabla \rho = \kappa \nabla^2 \rho, \quad (7.2)$$

$$\nabla \cdot \mathbf{u} = 0, \quad (7.3)$$

in $0 \leq z \leq L$. The simulated flow undergoes Coriolis acceleration but is constrained to be two-dimensional by taking $\partial/\partial y = 0$ for all dependent variables. The computational domain is L_x -periodic in the x -direction and stress-free rigid-lid boundary conditions are imposed at $z=0, L$. The equations are solved numerically using Fourier pseudo-spectral techniques and third-order Adams–Bashforth time stepping (Winters, MacKinnon & Mills 2004).

A stable linear density profile with constant N is prescribed along with an initial shear flow $\bar{U}(z)$ with constant shear S . Because the base flow is inconsistent with the stress-free boundary conditions, we modify it slightly so that, over relatively small regions of size $L/10$, the prescribed ambient shear decays smoothly to zero. In the interior of the domain, the ambient flow is uniformly sheared and stratified.

In the absence of additional perturbations, the prescribed flow $\bar{U}(z)$ simply oscillates at the inertial frequency f . (We consider only the parameter regime where the diffusion of the momentum associated with d^2U/dz^2 is negligible.) To examine the stability of initial flows parameterized by $(\mathcal{N}, \mathcal{S})$, the mass distribution is perturbed slightly at $t=0$. The perturbation ρ' takes the form

$$\rho' = W(z) \times \sum_{j=1}^4 \epsilon_j L \left| \frac{d\bar{\rho}}{dz} \right| \cos(k_j x + m_j z) \quad (7.4)$$

where ϵ_j is a small dimensionless random variable of $O(10^{-4})$, and the summation allows for random weighting of all sign combinations for the wavenumbers. The windowing function $W(z) = \exp -[z - L/2/\sigma]^2$ for $\sigma = L/5$ confines the perturbations to the interior region of interest and ensures that the displacements are identically zero at $z=0, L$.

Figure 6 shows the temporal evolution of the vertical velocity field at the point $(x, z) = (L_x/2, L/2)$ for the particular case $\mathcal{R} = 1/2$, $\theta/\pi = 0.3$ and $\phi/\pi = 0.15$ (see figure 2*b*). Also shown is an exponentially growing envelope function with growth rate $\mu \approx 0.1$ determined from the stability analysis. Linear stability analysis is only applicable while the amplitudes of the perturbations are small and it is apparent from the figure that the early growth is well-predicted theoretically but that later times are not.

Figures 7 shows snapshots of the density and perturbation vorticity fields as the perturbations grow from infinitesimal to finite amplitude. The times for these snapshots are indicated in figure 6. In the stability analysis, only the perturbation wavenumber ratio m/k is relevant. The vertical scale of the test wave is implicitly required to be small compared to a scale over which the ambient shear and stratification are approximately uniform. In this simulation, the vertical scale L is taken to be 10 m, the size of the computational domain, while the vertical

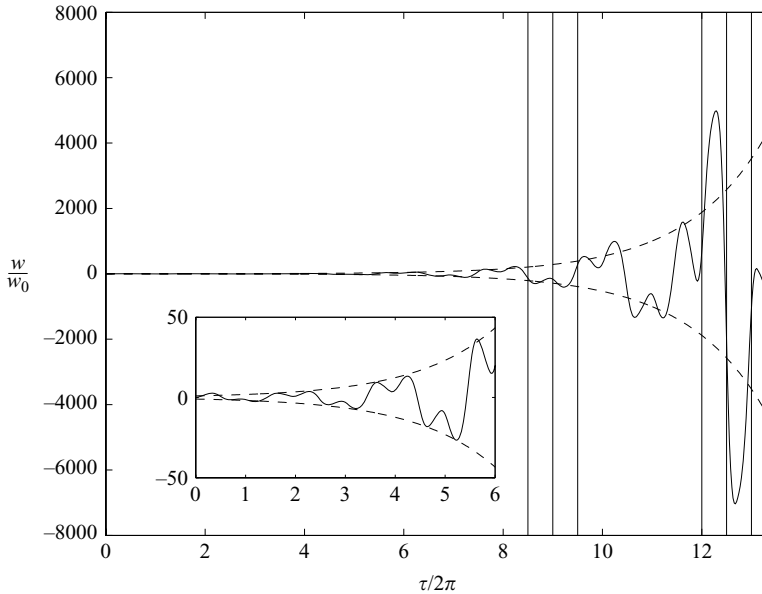


FIGURE 6. Time series of vertical velocity (solid) at $(x, z) = (L_x/2, L/2)$ for $\mathcal{R} = 1/2$, $\theta/\pi = 0.3$ and $\phi/\pi = 0.15$ (see figure 2*b*) along with exponential growth from linear stability analysis. Discrete time values for which snapshots of the density and perturbation vorticity fields are extracted are also indicated by vertical lines.

wavelength of the perturbation is set at 1 m. For $\phi/\pi = 0.15$, using $\tan \phi = m/k$ gives a horizontal wavelength of about 0.5 m. The imposed perturbation corresponds approximately to the most unstable mode for this particular weakly-stratified, rotating shear flow. At the times shown in figure 7(*a*), the perturbation appears wave-like in character.

At later times, figure 7(*b*), the perturbation has grown to finite amplitude and linear stability theory is no longer valid. The wave-like character of the flow is less evident and the flow field more closely resembles a network of interacting eddies. The flow is nonlinear during the time period spanned in the figure and, at times, the isopycnals are close to overturning. (Note the aspect ratio of the plots.) The detailed nature of the flow field in this regime is not of particular interest because of the two-dimensional approximation. Sheared flows with isopycnal overturns are often susceptible to three-dimensional gravitational instabilities which are not captured in these two-dimensional simulations. Nevertheless, based on the two-dimensional results, it seems reasonable to speculate that, given sufficient time to grow, the modes of instability identified here will lead to further instabilities and a transition to three-dimensional turbulence.

A second example, from the family of modes associated with T periodicity, is shown in figure 8(*a*). For this experiment, $\mathcal{R} = 10$, $\theta/\pi = 0.34$ and $\phi/\pi = 0.25$ (see figure 5). The growth rate for this mode is much faster and overturns are found after only three inertial periods. Again, careful exploration of the finite-amplitude limit requires three-dimensional simulations and is not pursued here. Finally, figure 8(*b*) illustrates a flow for which $N^2/S^2 < 1/4$ ($\mathcal{R} = 10$, $\theta/\pi = 0.4075$ and $\phi/\pi = 0.25$, see figure 5). In this flow, the instability grows very rapidly after only 2 inertial periods.

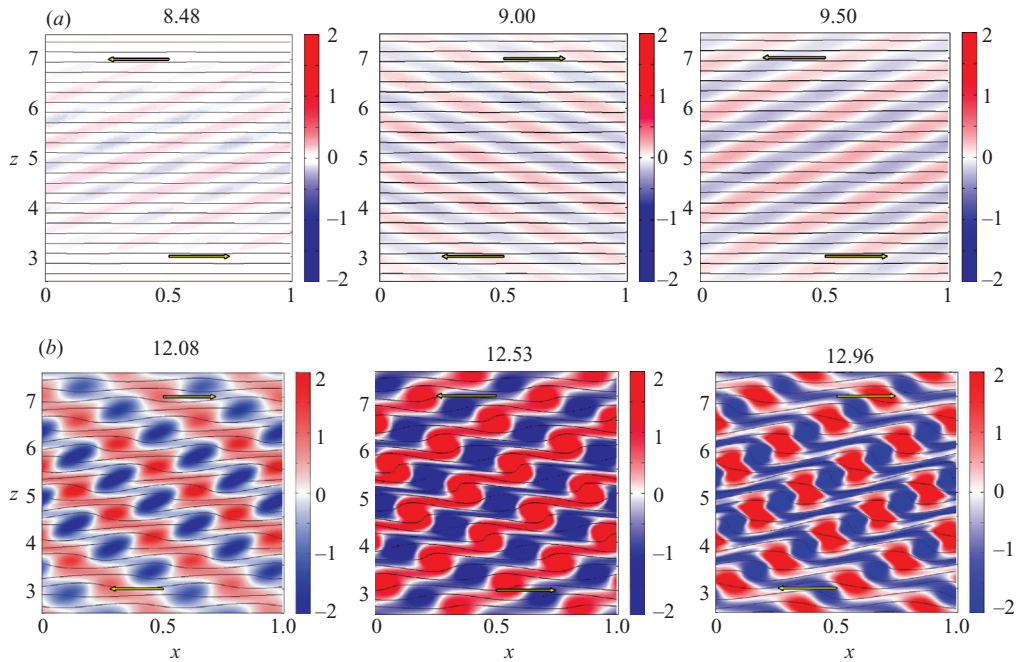


FIGURE 7. Density contours and perturbation vorticity $u'_z - w'_x$, normalized by the ambient shear S (a) during early stages of growth and (b) at later times for the case $\mathcal{R} = 1/2$, $\theta/\pi = 0.3$ and $\phi/\pi = 0.15$, (see figure 6). The arrows indicate the magnitude and direction of the inertial current $\bar{U}(z)$. The time in inertial periods $2\pi/f$ is shown above each panel.

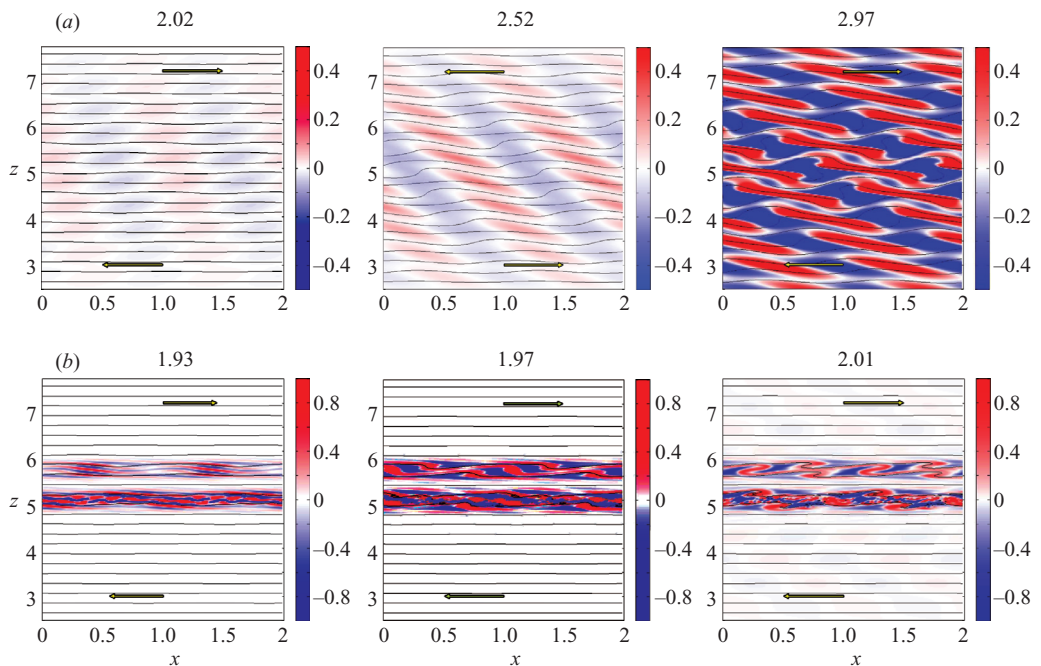


FIGURE 8. As in figure 8 for the cases $\mathcal{R} = 10$, $\theta/\pi = 0.25$ and $\phi/\pi = 0.34$ (a) and $\phi/\pi = 0.4075$ (b).

It is interesting to note the banded structure of the finite-amplitude state and the asymmetry about $z = L/2$ where the ambient flow $\bar{U} = 0$.

8. Conclusions

We conclude by listing the principal results derived from the linear stability analysis.

(i) Rapidly rotating sheared inertial currents, for which $N/f \leq 1/2$, are always unstable to inertia-gravity waves within a finite frequency band corresponding approximately to $\omega = f/2$ (figure 2).

(ii) Inertially oscillating shear flows are more unstable than steady flows in the sense that stable non-rotating flows with $N^2/S^2 > 1/4$ can be destabilized under the influence of rotation. Furthermore, for all values of \mathcal{R} , there are unstable modes with $N^2/S^2 > 1/4$, the condition for stability in steady stably-stratified shear flows.

(iii) For \mathcal{R} greater than $1/2$ and less than about 5 there exists at least some range of N/S for which the flow is stable to all perturbation wavenumber inclination angles ϕ (figure 4).

(vi) For \mathcal{R} greater than about 5, sheared inertial currents are always unstable for all finite values of N/S , with growth rates generally increasing with decreasing N/S (figures 4d and 5).

Because the inertial shear S and the ambient stratification N were both taken to be constants, independent of depth, it is implicit in the theory that the infinitesimal test waves parameterized by $\phi = m/k$ have vertical wavelengths that are small compared to any finite characteristic vertical scale of the background inertial current. In practice, if the characteristic scale of the inertial current is small, then the theory applies only to correspondingly smaller test waves. Viscous effects, which have not been included in the analysis presented here, will likely act to stabilize small-scale waves with linear inviscid growth rates μ less than $O(m^2\nu)$ where ν is the fluid viscosity.

The author gratefully acknowledges support from the US National Science Foundation (OCE04-25283) and the US Office of Naval Research (N00014-05-1-0513). The comments of Bill Smyth and two anonymous referees were very helpful and much appreciated.

REFERENCES

- BENDER, C. M. & ORSZAG, S. A. 1978 *Advanced Mathematical Methods for Scientists and Engineers*. McGraw-Hill.
- BENIELLI, D. & SOMMERIA, J. 1998 Excitation and breaking of internal gravity waves by parametric instability. *J. Fluid Mech.* **374**, 117–144.
- BOURUET-AUBERTOT, P., KOUDELLA, C., STAQUET, C. & WINTERS, K. B. 2001 Particle dispersion and mixing induced by breaking internal gravity waves. *Dyn. Atmos. Oceans* **33**, 95–134.
- BOURUET-AUBERTOT, P., SOMMERIA, J. & STAQUET, C. 1995 Breaking of standing internal gravity waves through two-dimensional instabilities. *J. Fluid Mech.* **285**, 265–301.
- CHANDRASEKHAR, S. 1961 *Hydrodynamic and Hydromagnetic Stability*. Dover.
- DRAZIN, P. G. 1977 On the instability of an internal gravity wave. *Proc. R. Soc. Lond. A* **356**, 411–432.
- DRAZIN, P. G. & REID, W. H. 1981 *Hydrodynamic Stability*. Cambridge.
- FARADAY, M. 1831 On the forms and states assumed by fluids in contact with vibrating elastic surfaces. *Phil. Trans. R. Soc. Lond.* **121**, 319–340.
- HOCHSTADT, H. 1961 *Special Functions of Mathematical Physics*. Holt, Rinehart and Winston.
- HOWARD, L. N. 1961 Note on a paper of John W. Miles. *J. Fluid Mech.* **10**, 509–512.
- INCE, E. L. 1956 *Ordinary Differential Equations*. Dover.

- LOMBARD, P. N. & RILEY, J. J. 1996 Instability and breakdown of internal gravity waves. i. linear stability analysis. *Phys. Fluids* **8**, 3271–3287.
- MAJDA, A. J. & SHEFTER, M. G. 1998 Elementary stratified flows with instability at large richardson number. *J. Fluid Mech.* **376**, 319–350.
- MIED, R. P. 1976 The occurrence of parametric instabilities in finite-amplitude internal gravity waves. *J. Fluid Mech.* **78**, 763–7xx.
- MILES, J. W. 1961 On the stability of heterogenous shear flows. *J. Fluid Mech.* **10**, 496–512.
- WINTERS, K. B., MACKINNON, J. A. & MILLS, B. 2004 A spectral model for process studies of density-stratified flows. *J. Atmos. Ocean. Tech* **21**, 69–94.